Table IV. Calculated Total Energies for GVB + CI Wave Functions of Peroxides and Peroxy Radicals

molecule	energy, hartree	molecule	energy, hartree
HOOH	-151.0216	HOO·	-150.3982
CH_3OOH	-190.0302	CH_3OO·	-189.4090
CH_3OOCH_3	-229.0391		

a 180° dihedral angle (staggered pairs on the two oxygens).

HO_2: The structure of HO_2

$R_0(OH) = 0.977$ Å $R_0(OO) = 1.335$ Å $\theta_0(OOH) = 104.1°$

is well established, having been obtained from microwave spectra of HO_2 and DO_2 by Beers and Howard.[15] In addition, many theoretical studies have been done on this molecule.[7-9,16-18] Our calculated structure (Table II)

$R_e(OH) = 0.972$ Å $R_e(OO) = 1.342$ Å $\theta_e(OOH) = 104.2°$

is very close to the experimental one, demonstrating the accuracy of our GVB + CI calculations, which include the resonance terms among the oxygen π orbitals. Of course, we calculate equilibrium parameters, whereas experimentally, these parameters are measured for the zero quantum level. Thus perfect agreement is not to be expected.

CH_3O_2. This is another case where no experimental data are available, and no previous ab initio calculations could be found. Structurally, CH_3OO is much like HO_2,

$R_e(CO) = 1.442$ Å $R_e(OO) = 1.339$ Å $\theta_e(OOC) = 110.2°$

The O-O bond lengths are essentially the same, and in both cases the OOR bond angle increases 4-5° from the corresponding peroxide (Table II). The C-O bond length is the same as in the methyl peroxides.

Summary

These calculations are the first reported ab initio studies of the equilibrium structures of CH_3OOH, CH_3OOCH_3, and CH_3OO. The calculated structural parameters of HOOH and HOO are very close to those obtained experimentally, demonstrating the accuracy of the GVB + CI approach.

The dihedral angles of the peroxides are calculated to vary from 119° in HOOH to 126° in CH_3OOH and 180° in CH_3OOCH_3, giving new insight into the gas-phase structures of peroxides.

Acknowledgment. We thank the U.S. Department of Energy for partial support of this work under Contract DE-AC03-76SF00767, Project Agreement DE-AT03-80ER10608.

Registry No. HOOH, 7722-84-1; CH_3OOH, 3031-73-0; CH_3OOCH_3, 690-02-8; HOO·, 3170-83-0; CH_3OO·, 2143-58-0; CH_3O·, 2143-68-2.

(15) Y. Beers and C. J. Howard, *J. Chem. Phys.*, **64**, 1541 (1976).
(16) A. Hinchliffe, *J. Mol. Struct.*, **66**, 235 (1980).
(17) T. H. Dunning, Jr., S. P. Walch, and M. M. Goodgame, *J. Chem. Phys.*, in press.
(18) D. H. Liskow, H. F. Schaefer III, and C. F. Bender, *J. Am. Chem. Soc.*, **93**, 6734 (1971).

Electron Nuclear Double Resonance (ENDOR) from Heme and Histidine Nitrogens in Single Crystals of Aquometmyoglobin

Charles P. Scholes,*[1a] Aviva Lapidot,[1b] Rita Mascarenhas,[1a] Toshiro Inubushi,[1c] Roger A. Isaacson,[1d] and George Feher[1d]

Contribution from the Department of Physics and Center for Biological Macromolecules, State University of New York at Albany, Albany, New York 12222, the Isotope Department, Weizmann Institute of Science, Rehovot, Israel, the Department of Biochemistry and Biophysics, University of Pennsylvania, Philadelphia, Pennsylvania 19174, and the Department of Physics, University of California at San Diego, La Jolla, California 92093. *Received July 6, 1981*

Abstract: Single-crystal ENDOR studies on the heme and proximal histidine nitrogens were carried out on magnetically dilute crystals of aquometmyoglobin. For some of this work heme nitrogens were enriched to about 90% in ^{15}N to give simpler ENDOR patterns than the ^{14}N heme crystals. ENDOR studies were done in three perpendicular planes determined by the heme normal and by the two mutually perpendicular heme nitrogen-nitrogen diagonals. The hyperfine and quadrupole tensors referred to these three directions were obtained for both heme and histidine nitrogens. We found, surprisingly, that diagonally opposite heme nitrogens were electronically not equivalent; i.e., their hyperfine couplings were *not* as expected by four- or twofold symmetry. This inequivalence was most dramatically shown by an approximate 5% difference in ENDOR frequencies within either relevant pair of nitrogens when the magnetic field was along heme nitrogen-nitrogen diagonals. In the orientation pattern near, but not at, the heme normal small variations were seen and were attributed to out-of-planarity of the heme. These variations enabled us to determine that the two nitrogens with larger spin density are on the pyrroles with methyl and propionic acid side chains, while the two nitrogens with smaller spin density are on pyrroles with methyl and vinyl side chains. The hyperfine couplings determined were related via standard ligand field techniques to unpaired electron density in nitrogen 2s and 2p valence orbitals. The primary covalent contributions to the hyperfine interaction arise from nitrogen-to-iron σ bonds. For an average heme nitrogen our analysis gave the percentages of unpaired 2s, $2p_\sigma$ and $2p_\pi$ electrons as 2.50, 5.6, and 0.9%, while on histidine nitrogen they were 2.92, 7.6, and 0.9%. The quadrupole couplings were analyzed and related to overall electron densities on nitrogen p orbitals. We have used spin Hamiltonian theory to examine the inequivalence of the heme nitrogens with the following results. (1) The measured inequivalence within a pair of heme nitrogens is due to a *real* electronic inequivalence, as opposed to an apparent inequivalence due to second-order effects in the spin Hamiltonian. (2) This real inequivalence arises from the large Fermi contact term in the spin Hamiltonian that is not required by the iron out-of-planarity. (3) The inequivalence can be explained by a small difference (~0.02 Å) in the bond distance to the iron between one heme nitrogen and its diagonally opposite partner.

The goal of this work was to obtain the electronic distribution at heme and histidine nitrogens in aquometmyoglobin. Magnetic resonance techniques are well suited for this purpose because electron nuclear hyperfine and quadrupole couplings show the

0002-7863/82/1504-2724$01.25/0

intimate electronic structure of molecules. When dealing with hyperfine couplings to nuclei like ^{15}N or ^{14}N, whose NMR sensitivity is low, electron nuclear double resonance (ENDOR) is the magnetic resonance technique of choice and was, therefore, used in this work.

Previous ENDOR on high- and low-spin ferric heme and heme proteins has been done on frozen solutions. In these samples, resolved ENDOR spectra were obtained at g value extrema that correspond to well-oriented subsets of molecules within the frozen solutions.[2-4] In particular, well-resolved couplings to heme and histidine nitrogens in aquometmyoglobin were first reported from frozen solution samples at the $g_{\parallel} = 2.00$ extremum,[5] corresponding to the normal of the heme plane. However, one cannot obtain well-resolved ENDOR spectra from frozen solutions of aquometmyoglobin at other g values such as those near g_x. $g_y \approx 6.00$ in the heme plane. In frozen solutions of aquometmyoglobin the magnetic field corresponding to a g value $\neq 2.0$ can lie at many different orientations with respect to the heme nitrogens and, therefore, gives rise to a poorly resolved, powder-averaged nitrogen ENDOR spectrum. Consequently, to obtain the complete, anisotropic hyperfine and quadrupolar tensors, ENDOR experiments on single crystals need to be performed. As has been shown earlier, magnetically diluted crystals are required for this purpose.[2,4]

We have reported preliminary ENDOR results from single crystals of metmyoglobin that contained naturally abundant [^{14}N]heme.[4] Although the spectra were very complex, they appeared to give evidence for an unexpected electronic inequivalence of heme nitrogens. ^{15}N, having a nuclear spin of $^1/_2$, gives fewer ENDOR lines than ^{14}N ($I = 1$). Thus, myoglobin prepared with [^{15}N]heme gave simpler spectra than did [^{14}N]heme and once again showed electronic inequivalence of the heme nitrogens. With the ^{15}N information in hand, we were able to return to the ^{14}N data and interpret it more fully.

We have referred our data and our spin Hamiltonian analysis to three heme-related orthogonal axes; these are the heme normal and the two nitrogen–nitrogen diagonal axes, shown in Figure 1. For a given heme nitrogen the two diagonal axes will be approximately in the heme plane along a Fe–N bond or perpendicular to it. The components of heme nitrogen hyperfine and quadrupole interactions along these axes have been determined in this work for the different heme nitrogens and compared to the parameters predicted from molecular orbital computations.

Materials and Methods

Materials. All common salts were Fisher ACS certified reagents or their equivalent. Sperm whale metmyoglobin, purchased in its lyophilized form from Sigma (type II), was used to prepare crystals that contained the naturally abundant ^{14}N heme. Metmyoglobin, dissolved in 0.02 M Tris (tris(hydroxymethyl)aminomethane) (pH 8.4), was first chromatographed on Whatman DE-52 as described previously.[5] Metmyoglobin was reduced with sodium dithionite (standard grade, Hardman & Holdman, Manchester, England) and converted to its diamagnetic carbon monoxy derivative by passing CO gas through it. Excess dithionite and its reaction products were removed by passing the protein through a column of Sephadex G-25-coarse with 0.1 M, pH 6.0 phosphate buffer as the eluant. The protein was reconcentrated to about 2.75 mM against Aquacide (Calbiochem, grade I) under a CO atmosphere. Myoglobin was then crystallized by the method of Kendrew and Parrish;[6] 9 mL of concentrated ammonium sulfate solution (Schwarz-Mann ultrapure, special-enzyme-grade ammonium sulfate, 760 mg/mL of H_2O) was added per 3 mL of 2.75 mM myoglobin solution. The latter contained carbon monoxy to aquomet forms in a 20:1 ratio. Crystallization beakers were placed in a CO-filled dessicator over alkaline pyragallol deoxidant. Diamond-shaped A-type ($P2_1$) crystals, 4 × 2 × 1 mm, were obtained within 2 weeks at room temperature. After the crystals were fully grown, they were stored in a CO-filled dessicator in a 4 °C cold room until ready for mounting.

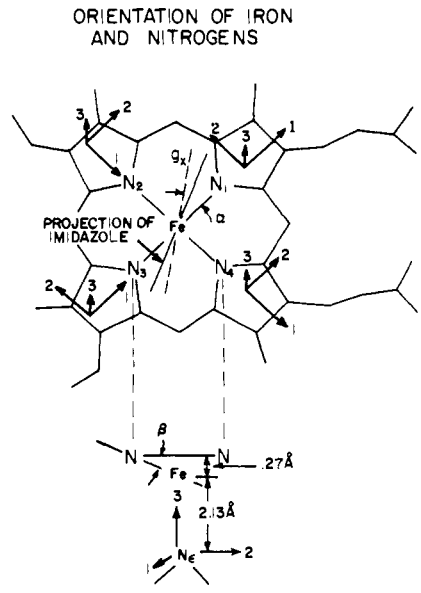

Figure 1. Orientation of the heme iron and its nitrogen ligands in metmyoglobin. Bottom part of figure represents edge view of heme plane. N_1, N_2, N_3, and N_4 are the heme nitrogens and N_ϵ is the histidine nitrogen. The axes labeled 1, 2, and 3 are the axes to which, for an individual nitrogen, we refer our hyperfine and quadrupole tensors. Angle $\alpha = 30°$ shows the rotation in the heme plane of the electronic g tensor with respect to the nitrogen axes. β is the out-of-plane angle, which is 7.6°.[13] Proceeding counterclockwise from N_1, the pyrrole groups which contain N_1, N_2, N_3, and N_4 respectively have the following as side chains: propionic, methyl; methyl, vinyl; methyl vinyl; methyl, propionic. In Figure 4 of Tokano's X-ray paper[13] our N_1, N_2, N_3, and N_4 would respectively belong to the pyrrole rings labeled IV, I, II, and III. The projection of the imidazole ring on the heme plane makes an angle of 19° rotated counterclockwise from the axis running from N_1 to N_3.

For reconstitution of [^{15}N]heme myoglobin, [^{15}N]protoporphyrin IX dimethyl ester was initially prepared at Rehovot in bacterial cultures of *Rhodopseudomonas spheroides* using the mutant 2-33R detailed in ref 7. These cultures were grown anaerobically in light on a medium enriched in δ-[^{15}N]aminolevulinic acid (91% ^{15}N) and [^{15}N]glycine (95% ^{15}N).[7b,c] The ^{15}N labeling of the porphyrin was determined by mass spectrophotometric analysis of the m/e 590 peak of the protoporphyrin IX dimethyl ester. The following isotopic enrichment was obtained: 91.8% total ^{15}N; $^{14}N_4$, 1.4; $^{14}N_3{}^{15}N$, 0.9; $^{14}N_2{}^{15}N_2$, 2.5; $^{14}N^{15}N_3$, 18.8; $^{15}N_4$, 76.3%.

Following hydrolysis of the ester, iron (90% enriched in ^{57}Fe) was inserted in the porphyrin by methods of ref 8, and the resultant hemin was inserted in apomyoglobin by methods of ref 9. Crystals were grown in a similar fashion to the ^{14}N-containing crystals.

Dr. Y. H. Wei, Department of Chemistry, SUNYA, kindly provided a frozen solution of beef heart myoglobin prepared by the method of ref 10.

The EPR/ENDOR Spectrometer. The basic EPR (electron paramagnetic resonance) and ENDOR apparatus used in this work has been

(1) (a) State University of New York at Albany. (b) Weizmann Institute of Science. (c) University of Pennsylvania. (d) University of California at San Diego.

(2) C. P. Scholes in "Multiple Electron Resonance Spectroscopy", M. M. Dorio and J. H. Freed, Eds., Plenum Press, New York, 1979, Chapter 8, pp 297–329.

(3) C. F. Mulks, C. P. Scholes, L. C. Dickinson, and A. Lapidot, *J. Am. Chem. Soc.*, **101**, 1645–1654 (1979).

(4) G. Feher, R. A. Isaacson, C. P. Scholes, and R. L. Nagel, *Ann. N.Y. Acad. Sci.*, **222**, 86–101 (1973).

(5) C. P. Scholes, R. A. Isaacson, and G. Feher, *Biochim. Biophys. Acta*, **263**, 488–452 (1972).

(6) J. C. Kendrew and R. G. Parrish, *Proc. R. Soc. London, Ser. A*, **238**, 305–324 (1958).

(7) (a) T. Hatch and J. Lascelles, *Arch. Biochem. Biophys.*, **150**, 147–153 (1972). (b) A. Lapidot and C. I. Irving, In "Proceedings of the Second International Conference on Stable Isotopes", E. R. Klein and P. D. Klein, Eds., Argonne, Illinois, 1975, USERDA 751027, p 427. (c) C. S. Irving and A. Lapidot, *J. Chem. Soc., Chem. Commun.*, 184 (1977).

(8) (a) T. Yonetani and T. Asakura, *J. Biol. Chem.*, **243**, 4715–4721 (1968). (b) T. Yonetani and T. Inubushi, Section II, Chapter III, in "Hemoglobins", In "Methods in Enzymology", E. Antonini, L. Rossi-Bernardi, and E. Chiancone, Eds., Academic Press, New York, to be submitted for publication.

(9) F. W. J. Teale, *Biochim. Biophys. Acta*, **35**, 543 (1959).

(10) I. Yamazaki, K. Yokota, and K. Shikama, *J. Biol. Chem.*, **239**, 4151–4153 (1964).

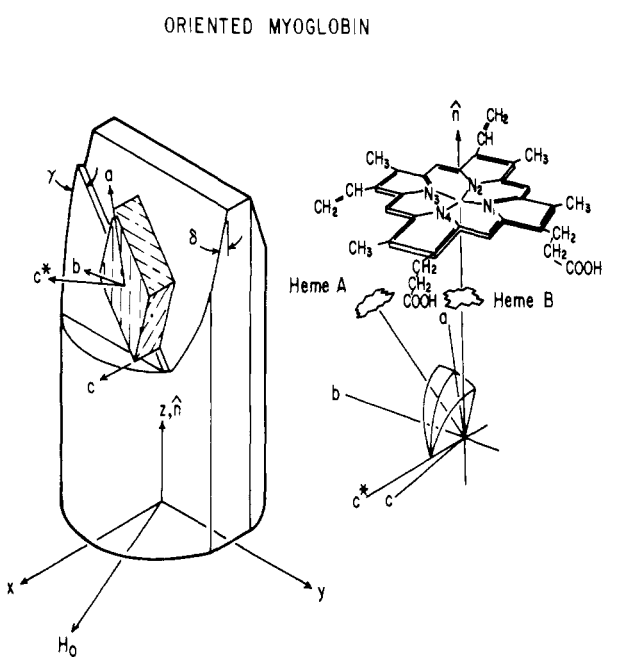

Figure 2. Sample pedestal used to rotate the myoglobin crystal about a heme normal. Height of the mount is 20 mm and diameter 8 mm. The z axis is along the vertical direction determined by the normal, $\hat{n}$, to the plane of heme B. The x and y axes are parallel to the nitrogen diagonals determined by N_2–N_4 and N_1–N_3 directions; the magnetic field lies in the x–y plane. This particular mount is based on Watson coordinates[12] with $\delta = 17°$ and $\gamma = 49°$. The right-hand side of the figure shows the two crystallographically inequivalent hemes B and A that are related by the $P2_1$ space group of myoglobin. Most ENDOR experiments were performed on the B heme, although an occasional check on the crystal orientation was performed by using the A heme.

described in ref 2. The microwave source and power supply were from a Varian V-4500 EPR system. The 100-KHz field modulation of about 5-G ptp (peak-to-peak) was used. The system was modified for low-power dispersion operation by the addition of a circulator and by-pass reference arm. A Varian F-8 NMR fluxmeter was used for magnetic field measurements. A Hewlett-Packard 5245L counter with 5257A transfer oscillator was used to measure the EPR frequency. The EPR-ENDOR cavity was a silvered quartz TE_{102} cavity similar in basic design to that shown in ref 11. RF (radio frequency) power was provided by an HP Model 8601A sweep generator driven by a linear voltage ramp from a Minicomputer (Nicolet, Model 1180). The RF power was amplified by an ENI (Electronic Navigation Instruments) Model 3100L, 100-W amplifier. RF fields of 6-Gauss ptp were used with a 10% duty cycle in order to prevent excessive RF-induced heating. Typically a range of 25 MHz was swept in 0.1 s, and the resultant RF-induced ENDOR signal was collected in the minicomputer signal averager. The experiments were performed at 2.1 K using a set of standard glass double Dewars. An ENDOR system based on a Bruker ER-420 system was used at Albany for several frozen solution measurements and for frequency modulated (FM) ENDOR.

Crystal Mounts. Single crystals were mounted inside 8-mm i.d. (inside diameter) quartz tubes on specially machined pedestals made either from quartz or Rexelite 1422 (Oak Materials, Gp., Laminates Div., Franklin, N.H.) (see Figure 2). Separate, specific pedestals were designed to rotate a crystal about a single vertical axis that either coincided with the heme normal so that the magnetic field would rotate in the heme plane or a nitrogen diagonal so that the magnetic field would rotate from the heme normal down to the other nitrogen diagonal. It was also important to be sure of the *sense* of the nitrogen diagonal that we rotated about. The major advantage of the pedestal mounts, compared to a two-axis rotator used in our early work, is that specific directions can be picked more readily and reproducibly. An example of a sample pedestal used for rotating one of the heme groups (labeled B) about its heme normal, $\hat{n}$, is shown in Figure 2. The rationale and procedure for making this mount are described in the supplementary material on microfilm. Pedestal modifications for rotating the crystal about N_{13} or N_{24} axes are available from the authors. ($\hat{n}_{13}$ and $\hat{n}_{24}$ are unit vectors along N_1–N_3 and N_2–N_4 directions.)

The 8-mm i.d. tube holding the crystal was attached to a stainless-steel tube that extended through the top of our cryostat where a goniometer was attached. Magnetic field rotations about the vertical axis were done either by rotating the vertical stainless-steel tube or by rotating the magnet on its base; the overall angular resolution was 0.2°. Errors in the direction of the crystal's vertical rotation axis were estimated at ±3°. They could arise either from improper mounting of the crystal on its pedestal or from errors in the published X-ray coordinates.[14a,b] To compensate for such errors and also to estimate them, a vertical coil was wound around the outside of the inner Dewar (2.5-in. o.d.). It produced a vertical magnetic field of up to 160 G and thereby tilted the effective magnetic field by several degrees.

Once the crystal was mounted, the large g anisotropy ($g_z = 2.00$, g_x, $g_y = 6.0$) was used to check its alignment. The mounts which rotated the crystal about the $\hat{n}_{13}$ or $\hat{n}_{24}$ axes should put the heme normal with its characteristic g value of 2.00 into the magnet plane. The deviation of the measured g values from 2.00 correspond to a misalignment of the heme normal out of the horizontal by less than 3°. Most of the ENDOR measurements were performed on the "B" heme (Figure 2). However, checks on crystal alignment were obtained by measuring g values from the crystallographically inequivalent "A" heme and comparing them to predicted g values of the A heme obtained from a knowledge of its orientation. The predicted g values of the A heme agreed well with A's experimentally measured g values and indicated misalignment of less than 3°. The measured g values at particular orientations agreed best with g values computed from the Watson coordinates.[12] However, mounts based on the Takano coordinates[13] or on preliminary EPR and ENDOR experiments gave satisfactory results. As an additional check, we computed ENDOR rotation patterns based on small 5° misalignments of the heme normal. These misaligned patterns differed markedly from our experimentally observed rotation patterns.

Methods of Data Analysis. The ENDOR spectra obtained along the nitrogen diagonal axes (Figure 3) and the heme normal (Figures 4 and 5) gave precise values for ENDOR frequencies. By using these values and the spin Hamiltonian discussed below, one obtained the hyperfine and quadrupole parameters (A and Q tensors) referred to these axes. In order to fit the ENDOR frequencies and rotation patterns (Figures 6–8) obtained at other orientations, a computer subroutine was used to diagonalize the general spin Hamiltonian (eq 2) at any orientation and to predict ENDOR frequencies. A modified[16,17] general multiparameter least-squares fitting routine[15] was used to obtain the best estimates of hyperfine and quadrupole parameters. This program used as input estimates the parameters obtained along the nitrogen diagonals or heme normal, the output parameters differed typically by less than 1% from the input parameters. The errors in the least-squares fitted parameters were obtained from the RMS (root mean square) error per point and from the "error" matrix which is inverted in the process of the least-squares fit.[18a] The fitted parameters and their errors are given in Table III. The errors are comparable to those computed from a number of separate ENDOR measurements done along the nitrogen diagonals and the heme normal. (See Table IIS, supplementary appendix for microfilm.)

Some data taken near but not at the heme normal indicated the need for an additional small hyperfine parameter reflecting the out-of-planarity of the heme, and it was included in some of our least-square fits. The statistical significance (goodness-of-fit) for including an additional parameter in the fitting procedure was obtained by using the "F test".[18b] This F statistic is determined from the sum of squares of errors between fitted and experimental points as computed for n or for $n + 1$ parameters. We considered the additional out-of-plane parameter to be significant when the F test showed less than a 1% probability that a random data set (as opposed to a set of data that truly depended on the additional

(11) H. L. Van Camp, C. P. Scholes, and R. A. Isaacson, *Rev. Sci. Instrum.*, **47**, 516–517 (1976).
(12) H. C. Watson, *Prog. Stereochem.*, **4**, 299–333 (1969).
(13) T. Takano, *J. Mol. Biol.*, **110**, 537–568 (1977).
(14) (a) H. Frauenfelder, G. A. Petsko, and D. Tsernoglou, *Nature (London)*, **280**, 558–563 (1979). (b) Recent measurements in ref 14a on the mean-square displacements of atoms within myoglobin crystals show that there is a 0.045-Å^2 mean-square variance in the position of the iron due to lattice distortion. If the same mean-square variance holds for heme nitrogens, then there is a ±0.21-Å uncertainty in a nitrogen coordinate along any particular direction. A pair of diagonally opposite nitrogens is about 4-Å apart, and the uncertainty of 0.21 Å in the position of a nitrogen translates into a 4° angular uncertainty in $\hat{n}$, $\hat{n}_{13}$, and $\hat{n}_{24}$.
(15) D. W. Marquardt, *J. Soc. Ind. Appl. Math.*, **11**, 431–434 (1963).
(16) J. H. Venable, Ph.D. Thesis, Yale University, 1965.
(17) C. P. Scholes, Ph.D. Thesis, Yale University, 1969.
(18) (a) P. R. Bevington, "Data Reduction and Error Analysis for the Physical Sciences", McGraw-Hill, New York, 1969, Chapter 11; (b) *ibid.*, Chapter 10.

Table I. Nitrogen ENDOR Frequencies (MHz) Measured in the Heme Plane Along N_1–N_3 and N_2–N_4 Directions[a-d]

H along N_1–N_3 direction (H = 1.10 kG, g = 5.91)		H along N_2–N_4 direction (H = 1.09 kG, g = 5.97)	
[^{14}N] heme myoglobin[a]	[^{15}N] heme myoglobin[b]	[^{14}N] heme myoglobin[c]	[^{15}N] heme myoglobin[d]
N_2: 8.12 ± 0.04, 8.56 ± 0.07, 9.02 ± 0.04 (N_4); 9.49 ± 0.06; 10.35 ± 0.10	10.22 ± 0.06, 11.18 ± 0.04 (N_ϵ); 12.59 ± 0.15 (N_ϵ); N_2: 13.42 ± 0.04, 13.98 ± 0.03, 14.71 ± 0.05 (N_4); 15.36 ± 0.03	N_3: 8.08 ± 0.12, 8.49 ± 0.13, 9.01 ± 0.15 (N_1); 9.39 ± 0.15	11.50 ± 0.07, 12.43 ± 0.05 (N_ϵ); N_3: 13.38 ± 0.09, 14.02 ± 0.09, 14.72 ± 0.07 (N_1); 15.36 ± 0.08
N_2: 11.16 ± 0.08, 11.54 ± 0.06, 12.16 ± 0.07 (N_4)	N_3: 19.23 ± 0.07, 19.98 ± 0.02, 20.70 ± 0.05 (N_1); 21.48 ± 0.03	N_3: 11.14 ± 0.14, 11.58 ± 0.10, 12.23 ± 0.17 (N_1)	N_2: 19.61 ± 0.04, 20.58 ± 0.06, 21.15 ± 0.03 (N_4); 22.02 ± 0.03
N_3: 12.60 ± 0.08, 13.27 ± 0.07, 13.77 ± 0.07 (N_1); 14.39 ± 0.07		N_2: 12.61 ± 0.11, 13.54 ± 0.12, 14.00 ± 0.19 (N_4); 14.74 ± 0.16	
N_3: 14.96 ± 0.10, 15.55 ± 0.09, 16.04 ± 0.07 (N_1); 16.53 ± 0.07		N_2: 15.26 ± 0.19, 15.90 ± 0.21, 16.29 ± 0.17 (N_4); 16.92 ± 0.19	

[a-d] Arrows show Zeeman pairs. For a free nitrogen nucleus the Zeeman term at a magnetic field of 1.1 kG used in these experiments, is $2^{14}g_n\beta_nH$ = 0.68 MHz and $2^{15}g_n\beta_nH$ = 0.95 MHz. The computed effective Zeeman terms (eq 3 for nuclear g values) are given as follows: *a*, for N_1 and N_3, $2^{14}g_{n1}\beta_nH$ = 1.12 MHz, for N_2 and N_4, $2^{14}g_{n2}\beta_nH$ = 0.98 MHz; *b*, for N_1 and N_3, $2^{15}g_{n1}\beta_nH$ = 1.56 MHz, for N_2 and N_4, $2^{15}g_{n2}\beta_nH$ = 1.36 MHz, for N_ϵ, $2^{14}g_n\beta_nH$ = 1.05 MHz; *c*, for N_1 and N_3, $2^{14}g_{n2}\beta_nH$ = 0.97 MHz, for N_2 and N_4, $2^{14}g_{n1}\beta_nH$ = 1.11 MHz; *d*, for N_1 and N_3, $2^{15}g_{n2}\beta_nH$ = 1.35 MHz, for N_2 and N_4, $2^{15}g_{n1}\beta_nH$ = 1.55 MHz, for N_ϵ, $2^{14}g_n\beta_nH$ = 1.03 MHz.

parameter) could have been equally well fitted by including the additional parameter.

Experimental Results

ENDOR Spectra. Most ENDOR frequencies are readily interpreted by first-order expressions resulting from hyperfine, quadrupole, and nuclear Zeeman interactions.[2,3] These expressions are given here to provide a background for understanding the observed spectra. To first order a set of magnetically equivalent ^{14}N (I = 1) nuclei gives four ENDOR transition frequencies at

$$^{14}\nu_{ENDOR} = \tfrac{1}{2}|^{14}A_{eff}| \pm {}^{14}\nu_N \pm \tfrac{3}{2}Q_{eff} \quad (1a)$$

and for ^{15}N ($I = {}^1/_2$) two ENDOR frequencies at

$$^{15}\nu_{ENDOR} = \tfrac{1}{2}|^{15}A_{eff}| \pm {}^{15}\nu_N \quad (1b)$$

where A_{eff} is the effective hyperfine coupling, Q_{eff} is the effective quadrupole coupling, and ν_N is the Larmor frequency (the Zeeman term) of the nuclei in the applied magnetic field. The predicted pairs of frequencies are separated by $2\nu_N = 2g_n\beta_nH$, where g_n is the nuclear g value (with possible pseudonuclear correction[19b]), β_n is the nuclear Bohr magneton, and H is the applied magnetic field.

Several orientations gave particularly distinct and information-rich spectra. One of these (Figure 3) occurred with the magnetic field in the heme plane along one of the nitrogen–nitrogen diagonals (and perpendicular to the other diagonal). The other orientation (Figure 4) occurred with the magnetic field along the g_z = 2.00 heme normal. The spectra of Figure 5 observed at g = 2.00 from frozen solutions of sperm whale myoglobin gave the same number of lines as Figure 4b and to within experimental error the same ENDOR frequencies. The spectrum observed from beef heart myoglobin was very similar.

In Figure 3 one group of ENDOR lines arises from the pair of heme nitrogens that have the magnetic field along their Fe–N bond and another group of lines arises from the pair of heme nitrogens which have the magnetic field perpendicular to the Fe–N bond. For the [^{15}N]heme a group of four lines was centered at 21 MHz and another group of four lines was centered at 15 MHz, thus, a total of eight [^{15}N]heme lines. For the [^{14}N]heme the higher frequency group of eight lines was centered near 15 MHz and the other group of eight lines near 10.5 MHz, thus, a total of 16 [^{14}N]heme lines. If diagonally opposite heme nitrogens were electronically equivalent, one would expect a total of *four* [^{15}N]heme and *eight* [^{14}N]heme ENDOR lines rather than double

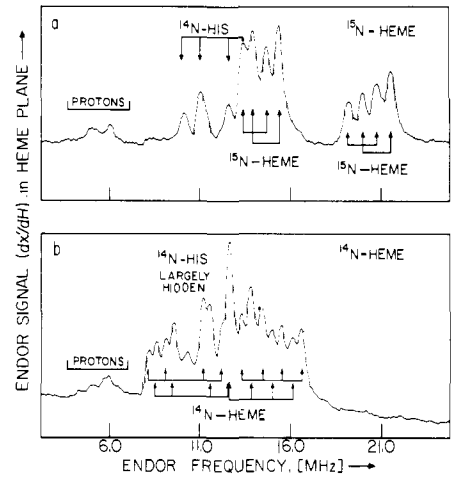

Figure 3. Nitrogen ENDOR signals at T = 2.1 K from heme and histidine nitrogens taken with the magnetic field in the heme plane along the nitrogen N_1–N_3 diagonal. Spectrum of Figure 3a was obtained with metmyoglobin prepared with 90% [^{15}N]heme, and in Figure 3b metmyoglobin contained 100% naturally abundant [^{14}N]heme. The ^{15}N pairs or the ^{14}N quartets belonging to the same nitrogen are indicated. Each spectrum was taken at an electronic g value near 5.9. The EPR frequency for Figure 3a was 9.09 GHz and for Figure 3b was 8.94 GHz. For other conditions see Experimental Section.

these numbers. The additional splitting of lines from diagonally opposite heme nitrogens amounts to 5% of their overall hyperfine couplings and is not an artifact of crystal misalignment. It occurred with all crystals and could be resolved within ±10° in any direction away from a diagonal. In the heme plane the splittings of Zeeman pairs were greater by about 50% than predicted from the intrinsic nuclear g values. This larger splitting was in good agreement with the large pseudonuclear[19b] contribution to the nuclear g value that is predicted to occur in directions perpendicular to the heme normal. A summary of the ^{14}N and ^{15}N ENDOR frequencies along the N_1–N_3 and N_2–N_4 directions (i.e., along $\hat{\mathbf{n}}_{13}$ and $\hat{\mathbf{n}}_{14}$ unit vectors) is given in Table I.

In Figure 4 the observed group of four [^{15}N]heme ENDOR lines and at least six (probably eight) [^{14}N]heme lines resulted from the nitrogen hyperfine and quadrupole couplings along the heme normal. If the heme nitrogens were electronically equivalent, then with the magnetic field along the heme normal, only two ^{15}N and four ^{14}N lines would be expected. Table II gives the ^{14}N and ^{15}N ENDOR frequencies and assignments measured along the heme normal at g = 2.00. The [^{14}N]heme lines near 2.4 and 4.4

(19) (a) A. Abragam and B. Bleaney, "Electron Paramagnetic Resonance of Transition Metal Ions", Clarendon Press, Oxford, 1970, Chapters 3.8, 4.2; (b) *ibid.*, Chapter 1.8.

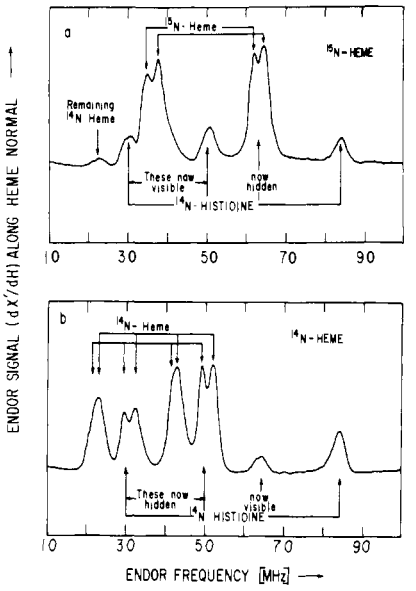

Figure 4. Nitrogen ENDOR signals from heme and histidine nitrogens taken with the magnetic field along the heme normal, $T = 2.1$ K. Spectra were taken at $g_z = 2.00$ and had EPR frequencies of 9.09 GHz for *a* and 9.08 GHz for *b*. Spectrum a is from a single crystal of [^{15}N]heme metmyoglobin. Spectrum b is from a single crystal of [^{14}N]heme metmyoglobin. Note that the combination of spectra a and b reveals all four [^{14}N]histidine ENDOR lines.

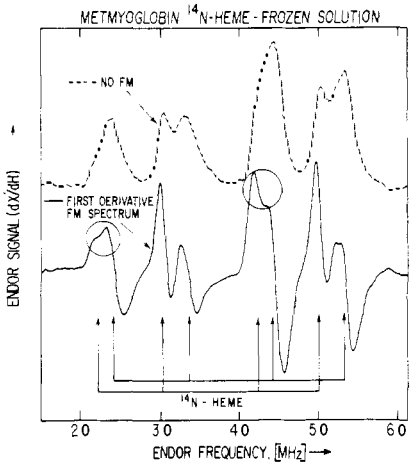

Figure 5. Comparison of conventional ENDOR (over the 1–6-MHz range that encompasses the [^{14}N]hemeENDOR) ENDOR) with the first derivative presentation obtained by frequency modulation. The spectra were from a frozen solution of 6 mM metmyoglobin in 1:1 glycerol–0.05 M phosphate buffer, pH 6.8. These two spectra were taken in order to resolve better the additional features of the [^{14}N]heme ENDOR, which are encircled. For frequency modulation, a sinusoidal frequency modulation, 0.1-MHz peak-to-peak, was used, and the modulation frequency was 90 Hz.

MHz were broader than the other [^{14}N]heme lines and exhibited hints of shoulders. To improve the resolution, we frequency modulated (FM) the ENDOR frequency to obtain the first derivative presentation of the conventional ENDOR signal. Figure 5 compares the first derivative signal of the heme nitrogens with their conventional ENDOR signal. The FM data showed that the two lines near 2.4 and 4.4 MHz were, indeed, composed of two components separated by ~0.2 MHz. Although the observed ENDOR lines at $g = 2.00$ did occur in pairs split by approximately the expected nuclear Zeeman splitting of $2\nu_n = 2g_n\beta_n H$ (with no pseudonuclear contribution at $g = 2.00$), small deviations from the expected Zeeman splittings were carefully noted. Notably, for both [^{14}N]heme and [^{14}N]histidine the splittings of the lower frequency Zeeman pair is greater than that of the corresponding higher frequency pair.

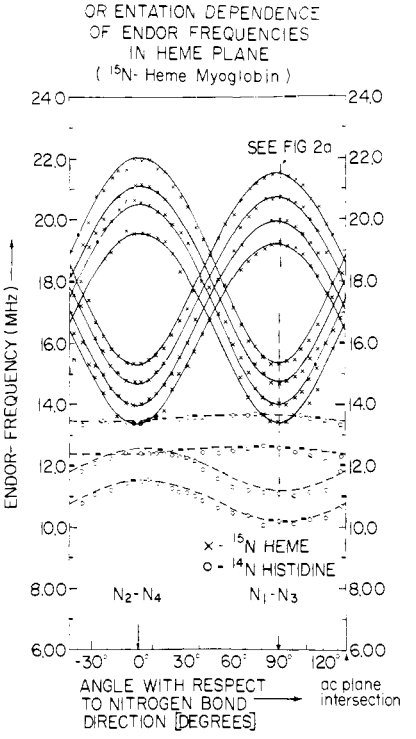

Figure 6. Orientation dependence of ENDOR frequencies in the heme plane from isotopically enriched [^{15}N]heme metmyoglobin. Solid lines are computer-generated curves obtained using a least-squares fit to the spin Hamiltonian of eq 2 and the parameters listed in Table III. EPR frequency was 9.08 GHz, the magnetic field ≈ 1.1 KG, and $T = 2.1$ K.

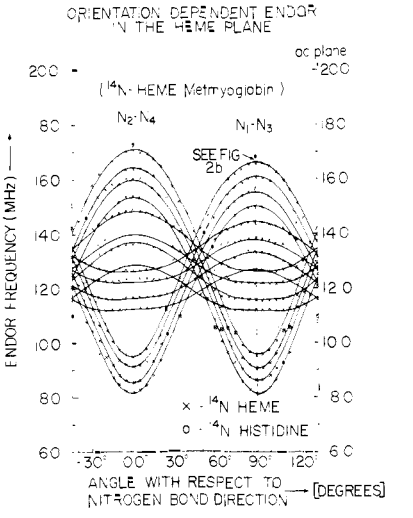

Figure 7. Orientation dependence of ENDOR frequencies in the heme plane from metmyoglobin containing [^{14}N]heme. Note the greater complexity and overlap compared to Figure 6. EPR frequency was 9.19 GHz, the magnetic field ≈ 1.1 KG, $T = 2.1$ K.

In both Figures 3 and 4, additional ^{14}N lines were observed from histidine; these lines were generally better resolved from the [^{15}N]heme crystals than from the [^{14}N]heme. The assignment of resonances to heme or to histidine was done by noting what resonances were left unchanged or were uncovered on going from [^{14}N]heme to [^{15}N]heme. The overall rotation patterns were also helpful in these assignments, as was previous work which compared myoglobin with hemins or mutant hemoglobins lacking a proximal histidine.[4]

A doubling of lines could, in principle, also occur if myoglobin existed in two different conformations. If this were the case, the ENDOR lines of histidine would also be expected to be split. This, however, was not observed. Additional evidence against two conformational populations is provided by the observations that

Table II. ENDOR Frequencies (MHz) Observed along the Heme Normal at $g = 2.00$ and $H = 3.24$ kG[a-c]

[^{15}N] heme[a]	[^{14}N] heme[b]	[^{14}N$_\epsilon$] His[c]
3.57 ± 0.04 (N_2:N_3)	2.16 ± 0.06	3.10 ± 0.05
3.87 ± 0.03 (N_2:N_3)	2.34 ± 0.03	5.16 ± 0.03
6.29 ± 0.04 (N_1:N_4)	3.02 ± 0.02 (N_2:N_3)	6.43 ± 0.05
6.55 ± 0.03 (N_1:N_4)	3.29 ± 0.03	8.42 ± 0.05
	4.22 ± 0.02	
	4.38 ± 0.02 (N_1:N_4)	
	5.00 ± 0.03	
	5.24 ± 0.04	

[a-c] Lines connected by arrows are nuclear Zeeman pairs, where $2|^{14}g_n\beta_n H| = 1.99$ MHz or $2|^{15}g_n\beta_n H| = 2.79$ MHz: *a*, obtained from single crystal [^{15}N] heme myoglobin. *b*, obtained from ENDOR on single crystal and frozen solution of [^{14}N] heme myoglobin (resolution of frequencies at 2.16 and 4.22 MHz obtained by frequency-modulated ENDOR on frozen solution); lines at 3.02 and 5.00 MHz were improperly assigned (albeit tentatively) in ref 5 to histidine; *c*, obtained from a combination of ENDOR results on ^{14}N and ^{15}N myoglobin.

different myoglobins (beef heart and sperm whale) as well as myoglobin samples prepared under different conditions (frozen solution and single crystals) gave the same ENDOR spectra at $g = 2.00$.

Detailed Orientation Patterns. Figures 6 and 7 show the orientation patterns for the nitrogen ENDOR frequencies as the magnetic field was rotated in the heme plane. The heme nitrogen pattern repeated approximately every 90° as we went from one nitrogen diagonal to the other. The N_1–N_3 and N_2–N_4 directions were determined with respect to the orientation at which the "A" and "B" heme planes of the $P2_1$ space group overlapped and also independently from the g values of the heme group.

ENDOR transitions along the N_2–N_4 directions (at ~22 MHz) are at a slightly higher frequency than the corresponding transitions along the N_1–N_3 direction. This effect is not due to a misorientation of the crystal but arises from a slight electronic inequivalence of adjacent heme nitrogens. In the [^{15}N]heme sample, the [^{14}N]histidine nitrogen ENDOR lines were easily followed and for the most part did not overlap with the lines from the heme. In the heme plane, the smaller hyperfine interaction and larger quadrupole interaction of the histidine were found near the N_1–N_3 axis (Figure 6), which is near the expected direction for the projection of the plane of the proximal histidine (Figure 1). (X-ray work[12] has indicated that the plane of the histidine is rotated counterclockwise by 19° from the N_1–N_3 axis toward N_2 so that the histidine plane would occur in Figure 6 at an angle of 109°.) The larger histidine hyperfine and smaller quadrupole interactions were found near the N_2–N_4 axis, approximately perpendicular to the plane of the histidine and near the expected direction for the histidine-to-iron π bonding.

Figure 8 shows the angular dependence of the ENDOR frequencies from the [^{15}N]heme as the magnetic field was rotated from the heme normal to the N_2–N_4 axis. Another similar pattern was obtained by following the ENDOR pattern from the heme normal down to the N_1–N_3 axis. From Figure 8 we see that most of the change in ENDOR frequencies occurs within ±30° of the heme normal. Although the overall pattern seems generally symmetrical about the heme normal (i.e., about 0° in Figure 8), a detailed investigation from ±6° to about ±20° from the heme normal revealed a slight asymmetry to the heme ENDOR patterns. That pair of diagonally opposite heme nitrogens (N_2 and N_4 in the case of Figure 8) for which the magnetic field was rotated from the heme normal to the magnetic axis near the Fe–N bond direction showed this asymmetric effect. Notably, at a given positive angle (like the +12° inset in Figure 8) its heme ENDOR lines were seen to be split, while at the corresponding negative angle there was only a single ENDOR line.

At the same time that we determined the orientation of hyperfine and quadrupole tensors, we also measured the orientation of the electronic **g** tensor and its principal values. We found g_x, g_y, and $g_z = 5.87$, 5.98, and 2.00, respectively, in agreement with earlier findings;[20,21] the g_x and g_y axes were rotated with respect to the N_1–N_3 and N_2–N_4 axes by 30° (see Figure 1).

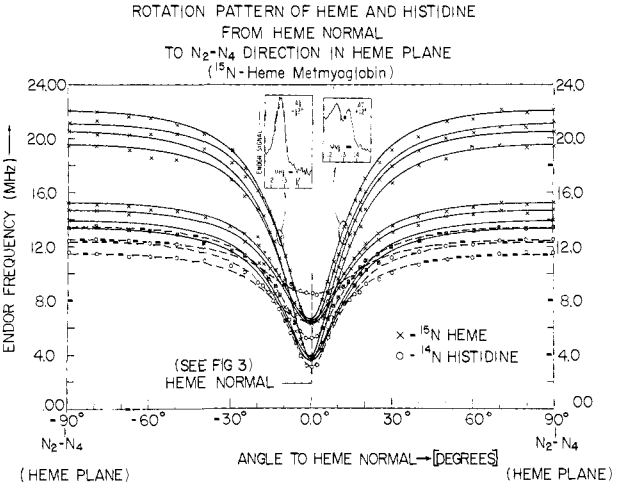

Figure 8. Orientation dependence of ENDOR frequencies in going from the heme normal to the N_2–N_4 direction in the heme plane for metmyoglobin containing [^{15}N]heme. EPR frequency was 9.08 GHz; the magnetic field was varied from 3.24 to 1.09 KG in going from $g = 2.00$ to $g \approx 6.0$. The inset figures show the highest frequency ENDOR lines observed at ±12° away from the heme normal. A split pair occurs for +12° and a single line for −12°. This effect is believed to be due to the out-of-plane character of the iron ($T = 2.1$ K).

Theory

Spin Hamiltonian. A standard spin Hamiltonian was used to analyze the nitrogen ENDOR results.[19a] For the overall ferric ground state ($S = {}^5/_2$) sextet, it has the form

$$\mathcal{H} = D[S_z^2 - \tfrac{1}{3}S(S+1)] + E(S_x^2 - S_y^2) + \beta_e H\cdot\mathbf{g}_e\cdot S + \sum_k\{[S_1A_{11}{}^kI_1{}^k + S_2A_{22}{}^kI_2{}^k + S_3A_{33}{}^kI_3{}^k + A_{13}{}^k(S_3I_1{}^k + S_1I_3{}^k)] + [I_1{}^kQ_{11}{}^kI_1{}^k + I_2{}^kQ_{22}{}^kI_2{}^k + I_3{}^kQ_{33}{}^kI_3{}^k + Q_{13}{}^k(I_1{}^kI_3{}^k + I_3{}^kI_1{}^k)] - \beta_n H\cdot\mathbf{g}_n{}^k\cdot I^k\} \quad (2)$$

where D and E are respectively the tetragonal and rhombic zero-field splitting parameters, $D = 9.26$ cm^{-1} [22] and $E/D \approx 0.0025$,[22,23] H is the applied magnetic field, and β_n and β_e are the electronic and nuclear Bohr magnetons, respectively. The electronic **g** tensor, $\mathbf{g}_e$, of the *overall* ferric sextet ground state is close to isotropic with $g_z = 2.00$ and $g_{x,y} = 1.98$.[23] The summation over k refers to the four heme and one histidine nitrogen. The first set of brackets in the summation describes the electron–nuclear hyperfine coupling, the second set of brackets the nuclear quadrupole coupling, and the last term in the summation describes the nuclear Zeeman interaction with the applied magnetic field. The axes to which we refer the nuclear spin Hamiltonian are shown in Figure 1. For a heme nitrogen, axis 1 points at or directly away from the opposite heme nitrogen and near to the Fe–N bond, axis 2 lies in the heme nitrogen plane perpendicular to axis 1, and axis

(20) E. F. Slade and R. H. Farrow, *Biochim. Biophys. Acta*, **278**, 450–458 (1972).
(21) M. Kotani, *Adv. Quantum Chem.*, **4**, 227–266 (1968).
(22) C. P. Scholes, R. A. Isaacson, and G. Feher, *Biochim. Biophys. Acta*, **244**, 206–210 (1971).
(23) P. Eisenberger and P. S. Pershan, *J. Chem. Phys.*, **45**, 2832–2835 (1966).

3 lies along the heme normal. Axes 1, 2, and 3 are approximately principal axes for the heme nuclear spin Hamiltonian and excellent fits to the ENDOR rotation patterns have been obtained by using only the parameters A_{11}, A_{22}, A_{33}, Q_{11}, Q_{22}, and Q_{33}. However, since the iron is slightly out of the plane of the four hemes (by about 0.27 Å),[13] axes 1 and 3 will not be precisely principal axes of the heme nitrogen spin Hamiltonian. Additional terms of the form $A_{13}^k(I_1S_3 + I_3S_1)$ for the hyperfine interaction and $Q_{13}^k(I_1I_3 + I_3I_1)$ for the quadrupole interaction, therefore, are required.

For the histidine nitrogens, one of the principal axes (axis 3) lies along the Fe–N_ϵ bond; the other two axes lie parallel to the plane of the four heme nitrogens in directions that are approximately parallel (axis 2) and perpendicular (axis 1) to the plane of the imidazole ring. The last term in the summation is the nuclear Zeeman interaction, which for the *overall* ferric electron spin sextet is approximately isotropic with $g_n = 0.403$ and -0.566 for ^{14}N and ^{15}N, respectively.

Because the zero-field splitting, D, is much larger than the electronic Zeeman splitting, EPR and ENDOR spectra are only observed from the ground $S_z = \pm^1/_2$ doublet of the sextet. In analyzing EPR and ENDOR data, it is, therefore, more convenient to convert eq 2 to an effective spin Hamiltonian that applies only to the ground-state doublet. The detailed Hamiltonian is given in the supplementary material on microfilm, and the solid curves in Figures 6, 7, and 8 are the result of a least-squares fit of the data to that Hamiltonian. Working in the $S_z = \pm^1/_2$ doublet has the following consequences. The true spin operator, S, in the electronic Zeeman and electron–nuclear hyperfine portions of eq 2 is replaced by the expression $^1/_2\mathbf{g}\cdot S'$, where $\mathbf{g}$ is the effective electronic $\mathbf{g}$ tensor and S' is the spin operator in the ferric *ground*-state doublet. The effective electronic g values are about three times larger in the heme plane than along the heme normal. Consequently, the effective hyperfine couplings in the heme plane are about three times larger than their true intrinsic values (A_{11}, A_{22}) given in Table III.[24a,b] Second, there will be an unusually large "pseudonuclear" contribution to the nuclear $\mathbf{g}$ tensor.[19b] [This is another way of saying that there will be a very large (of the order of 50%) chemical shift to the nuclear $\mathbf{g}$ tensor.] The pseudonuclear contribution arises because the S_x and S_y contributions to both the electronic Zeeman and magnetic hyperfine terms couple the ground $S_z = \pm^1/_2$ doublet to the next excited $\pm^3/_2$ doublet.[25] When taken to second order in perturbation theory, this coupling gives rise to a term that has the appearance of a nuclear Zeeman interaction. The expressions for the nuclear $\mathbf{g}$ tensor are[26]

$$g_{n1} = g_n + \frac{(g_x + g_y)\beta_e A_{11}}{3\beta_n D}$$

$$g_{n2} = g_n + \frac{(g_x + g_y)\beta_e A_{22}}{3\beta_n D} \qquad (3)$$

$$g_{n3} = g_n$$

Typical values of the nuclear $\mathbf{g}$ tensor are for [^{14}N]heme, g_{n1}, g_{n2}, and $g_{n3} = 0.665$, 0.586, and 0.403, respectively, and for [^{15}N]heme. g_{n1}, g_{n2}, and $g_{n3} = -0.929$, -0.815, and -0.566, respectively. These values were computed under the assumption that A_{11} and A_{22} are respectively positive for ^{14}N and negative for ^{15}N. The measured splittings in the heme plane, where the pseudonuclear shift is largest, are in agreement with the pseudonuclear correction to the nuclear g values and with these choices of signs for ^{14}N and ^{15}N.

Analysis of ENDOR Frequencies, Including Second-Order Effects. The observed ENDOR frequencies follow approximately the first-order expressions of eq 1. However, better estimates of the hyperfine and quadrupole parameters, including the sign of the latter, were obtained by including several second-order effects. The first of these is due to the fact that the external magnetic field is not infinitely large compared to the hyperfine field. Appropriate second-order expressions have been derived for the three principal axes. For general orientations the computer did the matrix diagonalization of eq 2, thereby implicitly taking account of the second-order effects. Taking H along the heme normal (axis 3), one obtains[27] for the ^{15}N

$$^{15}\nu_{ENDOR} = \tfrac{1}{2}|^{15}A_{33}| \pm [^{15}\nu_N - 9^{15}A_{22}{}^{15}A_{11}/(4\nu_e)] \quad (4a)$$

In this expression $^{15}\nu_N$ is the ^{15}N nuclear Zeeman splitting ($\sim$1.40 MHz) and ν_e is the microwave frequency ($\sim$9.1 GHz). Equation 4a theoretically predicts a decrease in the Zeeman splitting for a ^{15}N pair of $9^{15}A_{22}{}^{15}A_{11}/(2\nu_e) \approx 0.07$ MHz. The observed decrease from 2.79 to 2.70 ± 0.02 MHz was 0.09 ± 0.02 MHz in agreement with the theoretically predicted decrease.

For ^{14}N taking H along the heme normal, one expects two sets of Zeeman pairs labeled $^{14}\nu_{ENDOR}{}^+$, $^{14}\nu_{ENDOR}{}^-$, respectively, where

$$^{14}\nu_{ENDOR}{}^+ = \tfrac{1}{2}|^{14}A_{33}| + (Q_{11} - Q_{22})^2/[4(^{14}A_{33} \pm 2^{14}\nu_N)] - \tfrac{3}{2}Q_{33} \pm [^{14}\nu_N - 9(^{14}A_{11} - {}^{14}A_{22})^2/(8\nu_e)] \quad (4b)$$

$$^{14}\nu_{ENDOR}{}^- = \tfrac{1}{2}|^{14}A_{33}| + (Q_{11} - Q_{22})^2/[4(^{14}A_{33} \pm 2^{14}\nu_N)] + \tfrac{3}{2}Q_{33} \pm [^{14}\nu_N + 9(^{14}A_{11} + {}^{14}A_{22})^2/(8\nu_e)]$$

In these expressions $^{14}\nu_N$ is about 1.00 MHz. An important second-order effect noted from eq 4b is the perturbation on the measured ^{14}N Zeeman splittings by the terms in $(^{14}A_{11} \pm {}^{14}A_{22})^2/\nu_e$. These perturbations allow one to determine the *sign* of the quadrupole coupling, Q_{33}, which cannot be obtained from first-order ENDOR analyses. (If the sign of Q_{33} is known, the signs of Q_{11} and Q_{22} follow from the zero trace of the quadrupole interaction.[28]) In particular, if $^{14}A_{33} > 0$ (as is expected if the unpaired electron spin on the nitrogen is in a 2s valence orbital) and if $Q_{33} < 0$, the lower energy Zeeman pair, $^{14}\nu_{ENDOR}{}^-$, will have a larger splitting than the upper pair by $9(^{14}A_{11}{}^2 + {}^{14}A_{22}{}^2)/(2\nu_e) \approx 0.07$ MHz. As indicated from the ^{14}N ENDOR frequencies in Table II, the lower frequency ^{14}N Zeeman pair does indeed have a larger splitting than the higher frequency pair for both heme and histidine nitrogens. Thus the quadrupole coupling along the heme normal and along the Fe–N_ϵ bond for histidine is negative.

Another major correction for the ^{14}N ENDOR frequencies is the offset of the average ENDOR energy by the terms in $(Q_{11} - Q_{22})^2/[4(^{14}A_{33} \pm 2^{14}\nu_N)]$. To obtain the proper value of the ^{14}N ENDOR frequencies, we must subtract a number which is $(Q_{11} - Q_{22})^2/(2^{14}A_{33}) \approx 0.20$ MHz and better agreement between ^{14}N and ^{15}N hyperfine couplings is thus obtained.

Up to this point we have considered second-order effects from single nitrogens only. Second-order effects that might occur if there were an effective coupling between equivalent heme nitrogen nuclei are dealt with in Appendix I at the end of this paper. The calculated second-order splittings of this type were all <0.05 MHz, which is an order of magnitude smaller than the observed splittings. Thus we attribute the observed splittings in Figures 3–5 to an electronic nonequivalence of the heme nitrogens.

Estimate of the Hyperfine and Quadrupole Couplings from Ligand Field Theory. The hyperfine coefficients A_{ii} are related to the interactions with unpaired s and p nitrogen electrons and

(24) (a) C. P. Scholes, *J. Chem. Phys.*, **52**, 4890–4895 (1970); (b) R. Calvo, *J. Magn. Reson.*, **26**, 445–459 (1977).

(25) C. P. Scholes, R. A. Isaacson, T. Yonetani, and G. Feher, *Biochim. Biophys. Acta*, **322**, 457–462 (1973).

(26) In deriving the expressions for the pseudonuclear corrections in eq 3, we have neglected the electronic g_x, g_y anisotropy and have used an average electronic g value in the heme plane of $(g_x + g_y)/2 = 5.93$. The neglect of g_x, g_y anisotropy could lead to an error of about 0.4% in the theoretical expressions for g_{n1} and g_{n2}.

(27) The perhaps unexpected factor of 9 in these formulas is discussed in the supplementary material for microfilm.

(28) E. A. C. Lucken, "Nuclear Quadrupole Coupling Constants", Academic Press, New York, 1969, Chapters 7, 11.

(29) If the iron-to-heme nitrogen σ bond were taken as tilted back by an angle β so as to point more directly at the heme iron and if the heme nitrogen p_z orbital were also tilted back by β, then one might expect the following plausible changes in formulas 5a–d. The coefficients of A_σ in (5a) and A_π in (5c) would become $(3\cos^2\beta - 1)$ instead of 2; the coefficients of A_π in (5a) and A_σ in (5c) would become $-(1 - 3\sin^2\beta)$ instead of -1; a term in $(A_\sigma - A_\pi)$ would be added to A_{dd} in (5d).

with unpaired electrons on the metal by the following relations: For the heme nitrogen

$$A_{11} = A_{\text{Fermi}} + 3(\cos^2 \beta - 1)A_{dd} + 2A_\sigma - A_\pi \quad (5a)$$

$$A_{22} = A_{\text{Fermi}} - A_{dd} - A_\sigma - A_\pi \quad (5b)$$

$$A_{33} = A_{\text{Fermi}} - (1 - 3 \sin^2 \beta)A_{dd} + 2A_\pi - A_\sigma \quad (5c)$$

$$|A_{13}| = \tfrac{3}{2}(\sin (2\beta))A_{dd} \quad (5d)$$

For the histidine nitrogen

$$A_{11} = A_{\text{Fermi}} - A_{dd} - A_\sigma + 2A_\pi \quad (6a)$$

$$A_{22} = A_{\text{Fermi}} - A_{dd} - A_\sigma - A_\pi \quad (6b)$$

$$A_{33} = A_{\text{Fermi}} + 2A_{dd} + 2A_\sigma - A_\pi \quad (6c)$$

where A_{Fermi} is the Fermi contact term proportional to the unpaired electron density in nitrogen s orbitals, A_{dd} is the direct dipolar interaction with the electron spin on the iron, A_σ is the dipolar interaction with an unpaired electron in a nitrogen-to-iron p_σ orbital, and A_π is the dipolar interaction with an unpaired electron in the nitrogen p_π orbital perpendicular to either the pyrrole ring of the heme or to the imidazole ring of the histidine. (We neglect in-plane π bonding since the electrons that would be involved in such bonding are contained in a carbon-to-nitrogen orbital that is directed away from the metal.) β, the out-of-planarity angle, is 7.6°.[13] In eq 5a–d we have explicitly included the effect of the out-of-planarity of the iron on the direct dipolar terms.

We approximate the Fermi term by assuming that it arises only from unpaired electron spin density in the nitrogen 2s shell. We neglect all other contributions such as direct covalent overlap with nitrogens 1s[30] and core polarization and exchange terms.[31a-c] The Fermi contact interaction due to unpaired electron spin density in the nitrogen 2s orbital is

$$A_{\text{Fermi}}\ (\text{MHz}) = (8 \times 10^{-6}) f_s \beta_e \beta_n |\psi_{02s}|^2 \pi / (3hS) \quad (7)$$

where f_s is the fraction of an unpaired electron in a 2s orbital, ψ_{02s} is the 2s wave function at the nitrogen nucleus, and $S = {}^5/_2$. $|\psi_{02s}|^2 = 33.4 \times 10^{24}$ cm^{-3}.[32,33]

There is an anisotropic part of the hyperfine coupling that is related to the unpaired electron density by

$$A_p\ (\text{MHz}) = (2 \times 10^{-6}) f_p g_n \beta_n \beta_e \langle r^{-3} \rangle_{2p} / (5hS) \quad (8)$$

where f_p is the fraction of an unpaired electron in a particular p orbital and $\langle r^{-3} \rangle_{2p} = 21.1 \times 10^{24}$ cm^{-3} [32,33] is the expectation value of r^{-3} for a nitrogen p electron. Before we can compute the electron densities from A_σ and A_π, we need to extract the contribution of the direct dipolar coupling to the anisotropic hyperfine interactions. It is given by

$$A_{dd}\ (\text{MHz}) = 10^{-6} f_{Fe} g_n g_e \beta_n \beta_e / (R^3 h) \quad (9)$$

where R is the Fe–N distance and f_{Fe} is the fraction of the total spin residing on the iron. The fraction f_{Fe} was estimated in the following way: The hyperfine interaction of ^{57}Fe in metmyoglobin, which is due mainly to the Fermi contact interaction, was measured to be −27.16 MHz.[25] By comparing this value with that theoretically computed for free ferric ion (−39.24 MHz),[34] we deduce that 68% of the unpaired electrons (i.e., 3.4 e) reside on the iron. The measured contact interaction of the nearly ionic compound, K_2NaFeF_6, is −34.12 MHz;[35] the contact interaction of ^{57}Fe in metmyoglobin is 79% of this number. Theoretical calculations of the hyperfine coupling of ^{57}Fe in metmyoglobin predict that 63% of the unpaired electrons reside on the iron.[31b] Taking a value of 70% for f_{Fe}, we compute values of A_{dd} that are 0.47 MHz for [^{14}N]heme, −0.66 MHz for [^{15}N]heme, and 0.41 for [^{14}N]histidine. Using these values of A_{dd}, we compute from eq 5d A_{13} elements whose magnitudes are $|^{14}A_{13}| = 0.19$ MHz and $|^{15}A_{13}| = 0.26$ MHz.

The quadrupole couplings were interpreted by the Townes-Dailey (TD) model.[28,37] It is an approximate model that lends itself to simple, chemically intuitive bonding schemes. It is best suited for relating quadrupole parameters in similar chemical environments such as pyrrole nitrogens in heme and CuTPP (TPP = tetraphenylporphyrin). Although the absolute numbers may have a large error, useful trends of electronic populations in various valence orbitals may be obtained. Thus the quadrupole interaction, say, Q_{zz}, is related to the populations N_z, N_x, and N_y in p_z, p_x, and p_y orbitals by the relation $Q_{zz} \alpha [N_z - {}^1/_2(N_x + N_y)]$[30] and cyclically for x and y. The proportionality constant is found from the quadrupole coupling for a single electron in a p orbital.[28]

To use the TD approach, we use the following wave functions for the nitrogen orbitals

$$\psi_\pi = (2p_z) \quad \text{(population } a\text{)} \quad (10a)$$

$$\psi_{\sigma 1} = 1/\sqrt{2}[(2s)\sqrt{1 - \cot^2 \theta} - (2p_x)\cot \theta + (2p_y)] \quad \text{(population } b\text{)} \quad (10b)$$

$$\psi_{\sigma 2} = 1/\sqrt{2}[(2s)\sqrt{1 - \cot^2 \theta} - (2p_x)\cot \theta - (2p_y)] \quad \text{(population } b\text{)} \quad (10c)$$

$$\psi_{\sigma 3} = (2s)\cot \theta + (2p_x)\sqrt{1 - \cot^2 \theta} \quad \text{(population } c\text{)} \quad (10d)$$

where ψ_π is the π orbital with population a, $\psi_{\sigma 1}$ and $\psi_{\sigma 2}$ are the two σ orbitals, each with populations b directed at adjacent carbons, and $\psi_{\sigma 3}$ is the σ orbital with population c pointing at the metal. The CNC bond angle of 2θ is noted in Table Vb.

Using the wave functions given by eq 10, we obtain the principal elements of the quadrupole tensor Q_{11}, Q_{22}, and Q_{33}

$$Q_{11}/Q_0 = [c(1 - \cot^2 \theta) + b(\cot^2 \theta - \tfrac{1}{2}) - a/2] \quad (11a)$$

along Fe–N bond

$$Q_{22}/Q_0 = [-c/2(1 - \cot^2 \theta) + b/2(2 - \cot^2 \theta) - a/2] \quad (11b)$$

$\perp$ to Fe–N bond in heterocycle plane

$$Q_{33}/Q_0 = [-c/2(1 - \cot^2 \theta) - b/2(1 + \cot^2 \theta) + a] \quad (11c)$$

along π bond $\perp$ to heterocycle plane

where Q_0 is the proportionality constant relating the quadrupole parameters to electron density ($Q_0 = -4.5$ MHz).[28,30] Equation 11 holds for the heme nitrogens. For histidine, the Q_{33} component was measured along the Fe–N bond while the Q_{11} component was measured near the bond perpendicular to the heterocycle plane. Thus for histidine, subscripts 33 and 11 should be interchanged in eq 11.

Discussion

The Hyperfine and Quadrupole Tensors. Both the heme and histidine hyperfine tensors are approximately axial about their respective Fe–N bond directions. For the heme the difference between A_{22} and A_{33} is only 15% of the difference between A_{11} and the average of A_{22} and A_{33}. One would expect such an axial hyperfine tensor when the major anisotropic hyperfine interaction is from p_σ bonding to metal $d_{x^2-y^2}$ and d_{z^2} orbitals and when there is substantial direct dipolar interaction with unpaired electrons on the metal. The largest hyperfine couplings, A_{11} for heme nitrogen and A_{33} for histidine nitrogen, are thus along the re-

(30) T. G. Brown and B. M. Hoffman, *Mol. Phys.*, **39**, 1073–1109 (1980).
(31) (a) P. S. Han, T. P. Das, and M. F. Rettig, *Theor. Chim. Acta*, **16**, 1–21 (1970); (b) M. K. Mallick, J. C. Chang, and T. P. Das, *J. Chem. Phys.*, **68**, 1462–1473 (1978); (c) S. K. Mun, J. C. Chang, and T. P. Das, *J. Am. Chem. Soc.*, **101**, 5562–5569 (1979).
(32) D. R. Hartree and W. Hartree, *Proc. R. Soc. London, Ser. A*, **193**, 299–304 (1949).
(33) A. H. Maki and B. R. McGarvey, *J. Chem. Phys.*, **29**, 35–38 (1958).
(34) S. N. Ray, T. Lee, and T. P. Das, *Phys. Rev. B: Solid State*, **8**, 5291–5297 (1973).
(35) S. Hüfner and G. K. Wertheim, *Phys. Rev. B: Solid State*, **7**, 2333–2336 (1973).
(36) J. Owen and J. H. M. Thornley, *Rep. Prog. Phys.*, **29**, 675–728 (1966).
(37) C. H. Townes and B. P. Dailey, *J. Chem. Phys.*, **17**, 782–796 (1949).

Table III. Hyperfine and Quadrupole Couplings (in MHz)[a-c] from Complete Least-Squares Fit of all Data to Equation 2

	$^{15}A_{11}$	$^{15}A_{22}$	$^{15}A_{33}$	$^{15}A_{13}$ [c]	$^{15}A_{\text{Fermi}}$	$^{14}A_{11}$	$^{14}A_{22}$	$^{14}A_{33}$	Q_{11}	Q_{22}	Q_{33}
heme N_1	−14.02 ± 0.04	−9.81 ± 0.04	−10.27 ± 0.14	−0.06 ± 0.06	−11.37 ± 0.04	9.97 ± 0.02	6.97 ± 0.08	7.32 ± 0.10	−0.74 ± 0.04	1.08 ± 0.04	−0.34 ± 0.04
heme N_2	−13.63 ± 0.04	−9.43 ± 0.04	−9.87 ± 0.16	+0.29 ± 0.08	−10.98 ± 0.05	9.64 ± 0.20	6.78 ± 0.02	6.96 ± 0.18	−0.78 ± 0.04	1.01 ± 0.06	−0.23 ± 0.04
heme N_3	−13.50 ± 0.04	−9.44 ± 0.04	−9.73 ± 0.14	+0.36 ± 0.10	−10.89 ± 0.06	9.60 ± 0.02	6.73 ± 0.08	6.98 ± 0.10	−0.78 ± 0.06	1.06 ± 0.06	−0.28 ± 0.04
heme N_4	−14.27 ± 0.04	−9.92 ± 0.04	−10.35 ± 0.18	−0.25 ± 0.08	−11.51 ± 0.07	10.19 ± 0.12	7.07 ± 0.06	7.17 ± 0.20	−0.74 ± 0.04	1.00 ± 0.04	−0.26 ± 0.06
average of all four heme N	−13.86	−9.65	−10.06	—	−11.19	9.86	6.89	7.11	−0.77	1.04	−0.27
His N_ϵ						8.33 ± 0.04	8.08 ± 0.04	11.55 ± 0.10	0.31 ± 0.02	0.81 ± 0.02	−1.12 ± 0.04

[a] The axes 1, 2, and 3 for heme and histidine are described in the text. The nitrogen diagonal directions, N_2–N_4 and N_1–N_3, are respectively rotated by 19° away from the perpendicular to the histidine plane and away from the histidine plane itself. In the course of our fitting procedure, we did explicitly rotate the histidine 11 and 22 axes to where they might intuitively be expected (i.e., perpendicular and parallel to the histidine plane). Following such a rotation of axes, the resultant couplings were changed by a negligible amount from the results reported here and the RMS error per point difference between experiment and fit was about 40% larger. [b] The numbers given in this table were computed from the least-squares fit to the orientation data.[15-18b] For the [^{15}N]heme and [^{14}N]histidine, the data were obtained from rotations about the heme normal and about the two nitrogen diagonals. For the [^{14}N]heme the data were obtained from rotation about the heme normal and about the N_1–N_3 diagonal. Errors in parameters were computed from the RMS (fitted minus experimental) error per point of about ±0.15 MHz (coming primarily from off-axis points) and from the matrix that was inverted in the least-squares fit.[18b] [c] The F test for the significance of adding one more variable gave confidence levels for the addition of the $^{15}A_{13}$ term that were greater than 99% for N_2, N_3, and N_4 and about 99% for N_1.

spective Fe–N bonds. The difference between the other components indicates some rhombic character which can result from π bonding. Some rhombicity in the heme hyperfine tensor may also be due to out-of-planarity of the iron. The major contribution to the heme and histidine hyperfine tensors is isotropic. The average isotropic contribution to the heme nitrogen is 7.95 MHz for ^{14}N, −11.19 MHz for ^{15}N, and 9.31 MHz for the [^{14}N]histidine (Table IV). We can empirically compare the heme nitrogen hyperfine tensor with the tensor for the pyrrole nitrogens in CuTPP, given in Table IV. As indicated in eq 7 and 8, hyperfine couplings have an inverse dependence on the electron spin quantum number. S,[36] and so the magnitude of the ^{14}N hyperfine tensor from ferric heme is found to be about 5 times smaller than that of the nitrogens in CuTPP.[30]

Determination of Unpaired Electron Densities from Hyperfine Couplings—Comparison with Theory. With use of eq 7, the unpaired 2s electron densities shown in Table Va were computed. The theoretical treatment of ref 31c predicted Fermi terms that are about 70% of the experimental value for heme nitrogen and about 50% of the value measured for the histidine N_ϵ. Taking into account the difference in S, fairly similar values of the Fermi coupling of heme nitrogens in metmyoglobin and the porphyrin nitrogens of CuTPP are obtained. The major contributions in both cases must come from σ bonding (positive spin density) to the unpaired metal $d_{x^2-y^2}$ orbital.

By using eq 5 or 6 and the previously described values of A_{dd}, we calculated the unpaired electron densities in the p_σ and p_π orbitals (Table Va). The p_σ electron density is more than twice the s electron density in both heme and histidine Fe–N σ orbitals. If a simple sp^2 orbital scheme held, as outlined in eq 10, then we would predict a ratio of p to s electron of about 1 in the Fe–N σ orbital (eq 10d) where the CNC bond angle (2θ) is about 106°. On the other hand the molecular orbital treatment predicts a ratio of about 10.[31c] Reference 31c seems to overestimate by several fold the amount of p_σ and p_π covalency and as a result overestimates the anisotropic character (Table IV) of the hyperfine coupling. The overall p plus s spin density in the porphyrin σ orbitals is 25% greater in CuTPP than in the heme. This reduction in going from CuTPP to heme may reflect the shorter metal–porphyrin nitrogen distance in CuTPP[38] (1.98 vs. 2.04 Å) or the out-of-planarity of the heme iron. It has been pointed out that reverse donation of spin from a ligand orbital back to metal 4s can diminish the measured hyperfine coupling on a ligand.[36] This effect is most important when a metal, like high spin ferric iron, already has considerable unpaired spin. Thus, if such back donation were properly accounted for, even better agreement might be obtained between CuTPP and the heme nitrogen hyperfine couplings and spin densities. The small π contributions for both heme and histidine nitrogens need not be ascribed to the lesser covalency of π orbitals but conceivably to their delocalization over much of the porphyrin.

Inequivalence of Heme Nitrogens. The tetrapyrrole structure of heme suggests 4-fold (C_{4v}) symmetry at the heme iron with the concomitant electronic equivalence of all four nitrogens. If all four heme nitrogens had the same electronic distribution, then each nitrogen would have the same respective components of hyperfine and quadrupole couplings as its neighbors. However, a striking experimental finding of this work is that all four nitrogens are inequivalent. The inequivalence of diagonally opposite heme nitrogens was shown directly by the number of ENDOR lines in Figures 3, 4, and 5; the number was twice that expected from diagonally equivalent nitrogens.

From the ENDOR frequencies at other angles (Figures 6–8) we found that *all four* heme nitrogens were inequivalent. The least-squares fit (see parameters of Table III) shows that adjacent pairs of nitrogens are more similar than diagonally opposite pairs.

The major difference in hyperfine couplings between heme nitrogens is due to a ~5% difference in the Fermi interactions (i.e., in the unpaired nitrogen 2s electron densities) between di-

(38) E. B. Fleischer, C. K. Miller, and L. E. Webb, *J. Am. Chem. Soc.*, **86**, 2342–2347 (1964).

Table IV. Hyperfine and Quadrupole Parameters (MHz) for Heme[a] and Histidine Nitrogens: Comparison of Theory with Experiment

atom	A_{11}	A_{22}	A_{33}	A_{Fermi}	Q_{11}	Q_{22}	Q_{33}	ref
[^{15}N] heme (av of all four N's)	−13.86	−9.65	−10.06	−11.19				this work
[^{15}N] heme (theory)	−13.21	−4.64	−5.16	−7.67				31c, Mb-Hfs
[^{14}N] heme (av of all four N's)	9.86	6.89	7.11	7.95	−0.77	1.04	−0.27	this work
[^{14}N] heme (theory)	9.42	3.31	3.68	5.47	−1.10	1.79	−0.69	31c, Mb-Hfs
CuTPP porphyrin ^{14}N[b]	54.213 (10.84)	42.778 (8.56)	44.065 (8.81)	+47.019 (9.40)	−0.619	0.926	−0.307	30
[^{14}N] His	8.33	8.08	11.55	9.31	0.31	0.81	−1.12	this work
[^{14}N] His (theory)	2.70	2.70	8.18	4.53				31c

[a] Average values are listed. Nonequivalence of nitrogens was neglected (see Table III). [b] Values in parentheses have been divided by 5.

Table V

(a) s and p Spin Densities

atom	f_s,[a] %	$f_{p\sigma}$,[b] %	$f_{p\pi}$,[b] %
av of all four heme N's	2.5	5.6	0.9
His N_ϵ	2.9	7.6	0.9
CuTPP[30]	3.0	6.4	

(b) Estimate of Nitrogen Orbital Populations from Quadrupole Data

atom	2θ, deg	hybridization ratio,[c]	c pop. approx along nitrogen–metal bond	a pop. in π orbital	b pop. in C–N bond	N_T[d] total N pop.
av of all four heme N's	106	0.78	1.92	1.50	1.31	6.04
His N_ϵ	109.6	1.02	1.89	1.40	1.33	5.95
CuTPP	109	0.89	1.90	1.59	1.41	6.31

[a] Computed from eq 7 taking A_{Fermi} from Table IV. [^{14}N]- and [^{15}N] heme results were the same to within one part in 100. [b] Computed from eq 5 or 6, 8, and 9, taking $f_{Fe} = 0.70$ and taking values of A_{11}, A_{22}, and A_{33} from Table IV. [c] Given by $(\tan^2\theta - 1)$. [d] For a neutral nitrogen $N_T = 5.00$.

agonally opposite nitrogens. This difference is well outside experimental error. There also seems to be a larger p_σ density (by 10%) for the nitrogens that have the larger Fermi interaction. However, since the p_σ electron densities are related to relatively smaller experimental differences between hyperfine parameters, there would be a larger experimental error associated with the p_σ difference. There are some differences even between the nearly equivalent nitrogens; e.g., the **A** tensor values for N_1 are overall slightly less than N_4. Using the assignment of heme nitrogens based on their A_{13} term (discussed in the next section), we find that the nitrogens with larger hyperfine couplings (N_1 and N_4) are the ones that have propionic and methyl side chains, while the ones with smaller hyperfine couplings (N_2 and N_3) have vinyl and methyl side chains.

To provide insight into reasons for the heme nitrogen inequivalence, we considered two types of possible heme distortions. One is the well-known propensity of heme for doming or ruffling,[38,39] which would to first order leave the Fe–N distance unchanged. To estimate the effect on the hyperfine interaction, we made use of the chemically intuitive "angular overlap model".[40] For the heme nitrogens we found that a small change in the angular overlap with the $d_{x^2-y^2}$ orbital (as might arise from ruffling or doming) had little effect on the unpaired electron density at the nitrogen as long as bond lengths were kept constant. The reason is that other d orbitals with unpaired electron spin in them compensate for the diminished overlap to the $d_{x^2-y^2}$ orbital. In a more sophisticated approach we used an existing molecular orbital program for heme.[31,41] Small perturbations of the heme nitrogens by ±0.025 Å in a direction *perpendicular* to the Fe–N bond led as before to no change in the hyperfine coupling.

We next considered the effect of a small change in Fe–N bond length which might be more closely related to porphyrin core expansion[42] than to doming or ruffling. We calculated both the effect of such a change on hyperfine couplings and on the energy of the heme system. Displacements of ±0.025 Å *along* the Fe–N bond caused approximate ±5% changes in the Fermi interaction at the 2s heme nitrogen orbital of the perturbed nitrogen. The change in overall electronic energy of the system was ~100 cal (~6×10^{-3} eV) for a 0.025-Å displacement. This means that such distortions are energetically very feasible; indeed, they could contribute to the large number of conformational states that have been postulated to occur for heme in myoglobin.[43] (The variation in energy as a function of small heme nitrogen displacements indicated that we are near an energy minimum for our Fe–N bond length of 2.04 Å.) Thus, we suggest that differential displacements of ~0.02 Å could account for the difference in heme hyperfine couplings between heme nitrogens. The underlying cause of such displacements remains to be determined. The asymmetrically arranged heme side chains and the asymmetric protein environment could cause electronic distortions that could alter the Fe–N bond lengths. The calculations were performed on a heme that had only symmetrically placed protons on pyrrole substituents. It would be instructive to see if the proper protoporphyrin substituents could cause differences in the heme hyperfine couplings even if bond lengths were kept invariant.

Identification of Nitrogens from Out-of-Plane Effects. Insight into out-of-plane effects on the hyperfine Hamiltonian can be obtained by considering the point-dipolar interaction between an electron spin on the iron and a heme nitrogen nuclear spin. This interaction has the form

$$\mathcal{H}_{\text{dipole}}^{\text{point}} = [g_e\beta_e g_n\beta_n/(R^3h)][3(\vec{I}\cdot\vec{R})(\vec{S}\cdot\vec{R})/(R^2) - \vec{I}\cdot\vec{S}] \quad (12)$$

where $\vec{R}$ is the vector from the iron to the nitrogen. For a configuration shown in Figure 1, the spin axes 1 and 3 are neither perpendicular to nor colinear with the vector $\vec{R}$. Thus, there will be an out-of-plane term of the form $A_{13}(I_1S_3 + I_3S_1)$, where $|A_{13}|$ is given by eq 5d. The sign of A_{13} depends on the sign of the nuclear g value and has opposite sign for opposite nitrogens. $^{15}A_{13}$ is predicted negative for N_1 and N_4 and positive for N_2 and N_3. The noncolinearity of $\vec{R}$ and the spin axes causes a hyperfine tensor to be slightly rotated away from the axes 1 and 3 shown in Figure 1. In particular, for each heme nitrogen the principal axis along

(39) J. L. Hoard in "Porphyrins and Metalloporphyrins", K. M. Smith, Ed., American Elsevier, New York, 1975, pp 317–376.
(40) M. Gerlock and L. C. Slade in "Ligand Field Parameters", Cambridge University Press, New York, 1973, Chapter 8.
(41) S. K. Mun, M. K. Mallick, S. Mishra, J. C. Chang, and T. P. Das, *J. Am. Chem. Soc.*, **103**, 5024–5031 (1981).
(42) T. G. Spiro, J. D. Strong, and P. Stein, *J. Am. Chem. Soc.*, **101**, 2648–2655 (1979).
(43) R. H. Austin, K. W. Beeson, L. Eisenstein, H. Frauenfelder, and I. C. Gunsalus, *Biochemistry*, **14**, 5355–5373 (1975).

which the hyperfine coupling is a minimum will be slightly tilted toward the center of the heme away from the heme normal. The sense of the tilt will be opposite for opposite nitrogens. The effect of this tilt is to displace the ENDOR frequency minima of diagonally opposite nitrogens from each other. For example, in Figure 8 where the rotation axis is about the $\hat{n}_{13}$ direction, the frequency minimum for N_2 is shifted away from the heme normal by a small positive angle[44] and the minimum for N_4 away from the normal by a small negative angle.[44] If the hyperfine tensor is larger for N_4 than for N_2, then the effect of the tilt is to displace the frequency minima of these two nitrogens so that their curves are farther apart at small positive angles than at small negative angles; hence, there is splitting at +12° and no splitting at −12°. (Because g anisotropy enters, the effect is largest near but not at the heme normal.) If the major hyperfine coupling for N_4 had been less than for N_2, then the curves would have been farther apart at small negative angles. Similar arguments explained the behavior of nitrogens N_1 and N_3 when $\hat{n}_{24}$ was the rotation axis.

For ^{15}N, $^{15}A_{13}$ was the only out-of-plane parameter, and there was less interference from overlapping ENDOR resonances at angles near the heme normal where the effect of $^{15}A_{13}$ was largest. For ^{14}N, on the other hand, spectral overlaps with the larger number of ENDOR lines as well as an additional out-of-plane quadrupole term made the determination of $^{14}A_{13}$ more difficult. Although proper signs were in fact found for $^{14}A_{13}$ (which are opposite to those of ^{15}N because of the opposite sign of the nuclear g value), unwanted statistical correlation between the out-of-plane hyperfine ($^{14}A_{13}$) and the out-of-plane quadrupole (Q_{13}) parameters was obtained. The value of $^{15}A_{13}$ could in principle be used to obtain the distance by which the heme iron is out of the porphyrin plane. However, to quantitate the out-of-planarity, one would have to separate direct dipolar and covalent contributions to A_{13}. In our work we have found that the signs and average value of $^{15}A_{13}$ were in agreement with those predicted from the direct dipolar contribution to A_{13} given in eq 5d. The computed magnitude of $|^{15}A_{13}|$ is 0.26 MHz, as compared with the experimental average of 0.24 ± 0.12 (Table III). The values of $^{15}A_{13}$ for N_1 and N_4 are predicted and experimentally found to be negative and for N_2 and N_3 to be positive; this fact identifies N_1, N_2, N_3, and N_4.

If we neglect covalency, we obtain from the average magnitude of $|^{15}A_{13}|$ and from eq 5d an angle of $\beta \approx 7°$, i.e., an out-of-plane distance of 0.24 Å—in good agreement with the value of 0.27 Å obtained by X-ray[13] (see Figure 1).

Determination of the Electronic Populations in Nitrogen Orbitals from Quadrupole Couplings. Since the overall quadrupole tensor is traceless, we can compute only two independent quantities from the three expressions of eq 11. Thus, one of the quantities a, b, and c in eq 10 or 11 must be predetermined. If the $\psi_{\sigma 3}$ orbital interacts with the metal in both a bonding and an antibonding orbital, one can estimate c.[30] The antibonding orbital which contains the unpaired electron, contributes $f_s + f_\sigma$ electrons, while the bonding orbital contributes $2(1 - f_s - f_\sigma)$ electrons. Thus c was estimated to be equal to $2 - f_s - f_\sigma$, as given in Table Vb. A problem with this approach is that the directed σ orbital of $\psi_{\sigma 3}$ should have a hybridization ratio of unpaired p to s electrons of $(\tan^2\theta - 1) \approx 1$. The measured ratio of $f_{p\sigma}$ to f_s is found greater than 2.0. We consider the following possibilities: (i) use the crystallographic value of θ, compute c from the hyperfine data, and ignore the complication in hybridization ratio; (ii) use the measured hybridization ratio from the hyperfine data to compute an effective θ and use this same value of θ throughout eq 11; (iii) predetermine the orbital population, b, of the N–C directed $\psi_{\sigma 2}$ orbital (the population of this bond in heterocyclic nitrogen compounds, such as various pyridines,[45] is relatively insensitive to the other substituents on the nitrogens and typically has a value of 1.3[45,28]). Approaches i and iii gave very similar results for heme and histidine nitrogens. Consequently, we used results from these methods throughout this work.

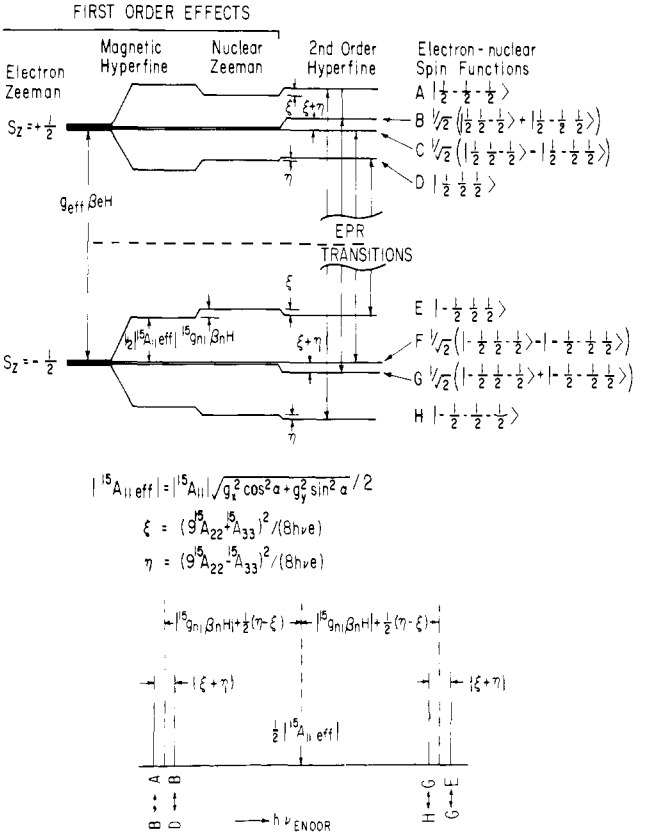

Figure 9. Energy levels (top) and ENDOR frequencies (bottom) of a system with an effective electron spin of $^1/_2$ interacting with two equivalent spin $^1/_2$ (^{15}N) nitrogens taken as N_1 and N_3. The magnetic field is along axis 1 (see Figure 1). The combined electron–nuclear eigenfunctions are indicated by $|M_s\,M_{I_1}\,M_{I_3}\rangle$. The contributions and splittings due to electron Zeeman, magnetic hyperfine, nuclear Zeeman, and second-order magnetic hyperfine are shown. (In accordance with the positive electron spin density on the nitrogen and the negative intrinsic nuclear g value, the signs of both $^{15}A_{11}$(eff) and $^{15}g_{n1}$ are taken as negative.) In the ENDOR technique EPR transitions are monitored while the nuclear transitions are induced. The four allowed nuclear transitions are caused by the ENDOR RF field along axes 2 or 3. These four transitions are centered at $^1/_2|^{15}A_{11}(\mathrm{eff})|$ and split off in pairs by $2|^{15}g_{n1}\beta_n H| + \eta - \xi$. There is a separation of each pair by the second-order splittings, $\xi + \eta$. The energy levels (left) are not drawn to scale since the EPR frequency is approximately 3 orders of magnitude larger than the other frequencies.

The orbital populations at various nitrogens, together with the overall electronic population, N_T, are given in Table Va. We are probably safest in comparing the similar heme and CuTPP nitrogens as long as the orbital populations have been computed in the same fashion. We find that there is less charge buildup on the heme nitrogen than on the CuTPP nitrogen. This may be because the more positively charged iron attracts away more nitrogen electrons and/or because some of the heme nitrogen electrons are effectively transferred to the histidine, whose population is increased above that found in imidazole. A more detailed comparison of electronic populations of heme and histidine-related heterocyclic compounds is given in the supplementary material on microfilm.

In molecular orbital work on hemin the quadrupole interaction was predicted from molecular orbital coefficients, using the TD approach. As shown in Table IV, the proper signs and ratios of quadrupole couplings were obtained from this theory, but the overall magnitudes of coupling constants are too large by about a factor of 2. The overall nitrogen population can be predicted at a nitrogen from the molecular orbital work on metmyoglobin.[31c] This population is 5.23 and 5.22 e for heme and histidine nitrogens, respectively, as compared with 6.04 and 5.95 e predicted from

(44) A positive rotation was a clockwise rotation of the crystal about the heme nitrogen's axis 2 which would take the magnetic field from alignment with axis 3 (heme normal) to alignment with axis 1.

(45) Y.-N. Hsieh, G. V. Rubenacker, C. P. Cheng, and T. L. Brown, *J. Am. Chem. Soc.*, **99**, 1384–1389 (1977).

the TD analysis of our experimental results.

Acknowledgment. We are grateful to Professor T. P. Das and Dr. K. Mishra for performing the molecular orbital calculations on heme in myoglobin where atomic coordinates were slightly perturbed. The work was supported by grants from the National Institutes of Health, No. AM-17884 (C.P.S.), No. GM-13191 (G.F.), No. 5507RR07122 (C.P.S.), and No. HL-14678 (A.L.) and the National Science Foundation Grant DMR 77-14657 (G.F.). C.P.S. is the recipient of an NIH Research Career Development Award 1 K04 AM00274.

Appendix. Second-Order Effects on the ENDOR Spectrum of Equivalent Nuclei

We compute here the second-order splittings due to couplings between electronically equivalent nitrogen nuclei. Such second-order effects have been seen by ENDOR of d^9 model CuTPP and AgTPP complexes that nearly possess the D_{4h} symmetry. We have assumed as a worst possible case that diagonally opposite heme nitrogens are equivalent. We estimate the magnitude of the splittings from the values of A_{11}, A_{22}, and A_{33} that we have found for [^{15}N]heme. For two equivalent ^{15}N nuclei interacting with an unpaired electron spin there are eight combined electron–nuclear spin states (shown in Figure 9); four of these have electron spin up and four of these have the electron spin down. Instead of having two transitions as predicted by eq 5a, there are four allowed transitions as shown in Figure 9. (These transitions are caused by the ENDOR RF field that is perpendicular to the externally applied field.) The splitting induced by second-order effects is given by $(9^{15}A_{22}^2 + {}^{15}A_{33}^2)/(4\nu_e) \approx 0.03$ MHz for the two nitrogens having the magnetic field along their axis 1 and $(9^{15}A_{11}^2 + {}^{15}A_{33}^2)/(4\nu_e) \approx 0.05$ MHz for the other two heme nitrogens having the magnetic field along their 2 axis.[27] (Second-order effects of the out-of-plane parameter A_{13} and of $g_x - g_y$ anisotropy along axis 1 or 2 are much less than these splittings.) The calculated splittings are an order of magnitude *less* than the observed extra, non-Zeeman splittings for [^{15}N]heme nitrogens. The [^{15}N]heme peaks of axis 1 near 21 MHz $\approx {}^1/_{4g_{eff}}{}^{15}A_{11}$ in Figure 3a have non-Zeeman splittings of about 0.85 MHz while those of axis 2 near 15 MHz $\approx {}^1/_{4g_{eff}}{}^{15}A_{22}$ have a non-Zeeman splitting of about 0.61 MHz.

For ^{14}N, because of the quadrupole splitting, there are 18 instead of eight combined electron–nuclear spin states for each pair of equivalent ^{14}N nuclei. We expect each pair of equivalent [^{14}N]heme nuclei to give four pairs (i.e., eight lines total) of ENDOR transitions with each pair centered at a frequency predicted by an equation like eq 5b. We have computed the splittings within an individual pair and have found them to be $(9^{14}A_{22}^2 + {}^{14}A_{33}^2)/(2\nu_e) \approx 0.03$ MHz for the two nitrogens that have the magnetic field along axis 1 and $(9^{14}A_{11}^2 + {}^{14}A_{33}^2)/(2\nu_e) \approx 0.05$ MHz for the two nitrogens that have the magnetic field along axis 2. Again, these splittings are an order of magnitude less than the observed splittings for the [^{14}N]heme nitrogens. The [^{14}N]heme peaks of axis 1 centered near ${}^1/_{4g_{eff}}{}^{14}A_{11} \approx 15$ MHz in Figure 2b have a non-Zeeman ${}^1/_{4g_{eff}}{}^{14}A_{11}$ of about 0.68 MHz while the [^{14}N]heme peaks of axis 2 centered near ${}^1/_{4g_{eff}}{}^{14}A_{22} \approx 10.5$ MHz have a non-Zeeman splitting of about 0.41 MHz. We note that the overall ratio of the observed non-Zeeman inequivalences for ^{15}N and ^{14}N is approximately the ratio of the magnitudes of ^{15}N to ^{14}N nuclear g values (i.e., 1.40). Thus, as stated in the text, we attribute the observed splittings to an electronic inequivalence of heme nitrogens.[46]

Registry No. Heme, 14875-96-8; histidine, 7006-35-1.

Supplementary Material Available: (a) A more detailed explanation and rationale for the sample mounting pedestal, (b) the detailed spin Hamiltonian referred to the ground $S_z = \pm{}^1/_2$ doublet of the overall ground $S = {}^5/_2$ sextet, (c) a detailed comparison of electronic population derived from quadrupolar data on nitrogen heterocycles related to heme and histidine; also a table (Table IS) that gives the quantitative electronic population related to item c; also a table (Table IIS) that gives hyperfine and quadrupole couplings directly computed only from ENDOR data taken along axes 1, 2, or 3 (6 pages). Ordering information is given on any current masthead page.

(46) In the case where all four heme nitrogens are equivalent and the magnetic field is along the heme normal, the problem becomes considerably more difficult than the problem of two magnetically equivalent nitrogens. There would be 32 ^{15}N or 162 ^{14}N combined electron–nuclear states. Having unambiguously found that a first-order inequivalence of hyperfine couplings readily accounts for the simpler case with two nitrogens, we did not proceed with the four nitrogen exercise. However, if nitrogens were equivalent only in pairs when the magnetic field was along the heme normal, then the theory which we have worked out for equivalent pairs would predict second-order splittings ~0.07 MHz for both [^{15}N]heme and [^{14}N]heme.

Determination of the Orientation of Adsorbed Molecules at Solid–Liquid Interfaces by Thin-Layer Electrochemistry: Aromatic Compounds at Platinum Electrodes

Manuel P. Soriaga and Arthur T. Hubbard*

Contribution from the Department of Chemistry, University of California, Santa Barbara, California 93106. *Received December 22, 1980*

Abstract: Accurate measurements of the limiting coverages of adsorbed molecules on smooth platinum electrodes are reported. Comparison of measurements with values calculated for various possible molecular orientations indicates the predominant orientations of the adsorbed molecules. Experimental data were obtained by linear potential scan voltammetry and potential-step chronocoulometry using thin-layer electrodes. Calculations were based upon covalent and van der Waals radii as tabulated by Pauling and were tested against the results of classical adsorption experiments. Forty compounds were studied, representing a wide range of structures and chemical properties: simple diphenols and quinones; alkyl-substituted diphenols and quinones; dihydroxybenzaldehydes; halogenated diphenols and quinones; polyhydroxybenzenes and quinones; hexaoxocyclohexane; N-heteroaromatics; diphenols having surface-active side chains; polycyclic diphenols and quinones. The most probable orientation was determined for each adsorbed compound.

Introduction

Methods to determine the orientation of an adsorbed molecule have been sought for a long time. Some progress toward this objective, at least at solid surfaces in ultra-high vacuum, has been reported by using methods based upon electron and neutron diffraction and electron spectroscopy.[1,2] Also, there is an excellent

0002-7863/82/1504-2735$01.25/0